LIMNOLOGY and OCEANOGRAPHY

ASLO

Limnol. Oceanogr. 70, 2025, 3696–3710

doi: 10.1002/lno.70226

RESEARCH ARTICLE

Quantifying nutrient supply to the eddy-influenced subtropical North Pacific upper ocean: Modified optimum multiparameter analysis using rare earth elements from three GEOTRACES cruises

Siteng J. Zhu [1], **Jing Zhang,** [1,2*] **Qian Liu,** [2] **Alan M. Shiller,** [3] **Chuanjun Du,** [4] **Zhimian Cao,** [5] **Xianghui Guo** [5], **Yihua Cai,** [5] **Xin Liu** [5]

[1]Faculty of Science, University of Toyama, Toyama, Japan; [2]Frontiers Science Center for Deep Ocean Multispheres and Earth System, and Key Laboratory of Marine Chemistry Theory and Technology, Ministry of Education, Ocean University of China, Qingdao, China; [3]School of Ocean Science and Engineering, University of Southern Mississippi, Stennis Space Center, Mississippi, USA; [4]State Key Laboratory of Marine Resource Utilization in South China Sea, Hainan University, Haikou, Hainan, China; [5]State Key Laboratory of Marine Environmental Science and College of Ocean and Earth Sciences, Xiamen University, Xiamen, China

Abstract

Horizontal/Vertical nutrient supply in the upper ocean of the North Pacific Subtropical Gyre (NPSG) plays a pivotal role in biogeochemical cycling and CO_2 uptake. However, research quantifying water/nutrient transport based on direct chemical observations and measurements is limited. Based on observations made during three GEOTRACES cruises in spring, summer, and winter, we identified horizontal and vertical water sources and quantified the water and nutrient supply, applying modified Optimum Multiparameter (OMP) analysis based on iterative calculation, in which rare earth elements (REEs) were used as quasi-conservative chemical tracers. The mean quantification results with a depth of ≤ 200 m show that Equator-derived water (Nutrient fraction: 51% ± 37%) and vertical supply (31% ± 33%) are the dominant nutrient sources; northern NPSG-derived water (0% ± 1%) has little influence; North Equatorial Current-derived water shows a higher contribution at 200–300 m (38% ± 26%) than the shallow layers (10% ± 19%); coast-derived water (7% ± 15%) contributes to NPSG in an inconsistent way. In addition, the enhanced vertical nutrient supply during the sampling period, which is more significant in spring, is likely to be attributed to the influence of what are considered different types of eddies based on the sea surface height. The vertical fluxes of dissolved inorganic nitrogen in the bottom euphotic layer at stations near warm, cold, and no eddies were estimated to be 0.10–0.76, 0.21–2.13, and 0.066–0.53 mmol m^{-2} d^{-1}, respectively, which are 1–100 times the supply from nitrogen fixation. These nutrient fluxes could explain 5–169 mg C m^{-2} d^{-1} of the carbon fixation in the euphotic zone.

Horizontal and vertical nutrient supply in the upper North Pacific Subtropical Gyre (NPSG) regulates biogeochemical cycles and CO_2 uptake. The NPSG functions as a significant CO_2 sink in the North Pacific (Takahashi et al. 2009), despite concurrently constituting the world's largest oligotrophic marine desert with chronically depleted surface nutrients and low chlorophyll concentrations (Karl et al. 1997; Karl and Church 2017; Meng et al. 2021). Mesoscale eddies (cold/warm-core systems) are widely distributed in the southwestern NPSG (Chen et al. 2021; Cheng et al. 2014), providing a major pathway for nutrient transport from nutrient-rich subsurface water to the surface (Falkowski et al. 1991; Chelton et al. 2011; Radic et al. 2011) and thus affecting biological processes and carbon export (McGillicuddy et al. 1998; Resplandy et al. 2019; Zhou et al. 2021). Model analysis by McGillicuddy and Robinson (1997) suggests that mesoscale eddies may be the dominant mechanism supplying nutrients to the euphotic zone of the oligotrophic ocean, delivering 0.35 ± 0.10 mol nitrogen m^{-2} yr^{-1} through a mechanism they name eddy pumping. Within a warm eddy near Station ALOHA, chlorophyll concentrations in the near-surface ocean were ~ 5-fold greater than in the surrounding waters (Fong et al. 2008).

*Correspondence: jzhang@sci.u-toyama.ac.jp

Associate editor: Phyllis Lam

However, few relevant quantitative data have been reported on the composition of NPSG water and nutrient supply, with this sparsity of data the result of the large spatio-temporal variability in the physical characteristics associated with eddies (Barone et al. 2022). Moreover, identification of water masses using chemical tracers remains challenging due to the complex water composition in the region, including horizontal advection (e.g., North Equatorial Current, northern NPSG water, Coastal water, Equatorial water) and vertical mixing.

In recent years, novel tracers, particularly trace elements, have been employed to enhance water composition identification and mixing quantification (Chen et al. 2013; Kumamoto et al. 2018; Whitmore et al. 2020). Zhang et al. (2018) demonstrated the utility of heavy rare earth elements (REEs) as semi-conservative tracers for water mixing studies, based on their long oceanic residence times ($\sim 10^3$ yr, Alibo and Nozaki 1999), despite minor particle scavenging effects (Byrne and Kim 1990). Applications include quantifying oxygen-depleted water in the East China Sea (Liu et al. 2022) and Atlantic Ocean mixing regimes (Zheng et al. 2016). Beyond REE concentrations, anomalies (e.g., Ce/Ce*, Eu/Eu*) and ratios (heavy/light REEs [HREE/LREE], Y/Ho) provide insights into mixing dynamics and biogeochemical processes like phytoplankton blooms and weathering (Nozaki et al. 1997; Hara et al. 2009; Möller et al. 2021). For example, the Ce deficiency (low Ce/Ce*) in seawater is subject to preferential scavenging over REEs due to the oxidation of Ce(III) to Ce(IV) (Moffett 1990), while HREE/LREE ratios indicate particle adsorption biases favoring light REEs (Zhang et al. 2008). Compared to widely used tracers like potential temperature and salinity, REEs effectively increase the number of tracers and improve source discrimination through concentration and pattern analyses. Additionally, REE analysis requires significantly smaller sample volumes (10–100 mL; Hatje et al. 2014; Behrens et al. 2016) compared to conventional isotopic tracers (e.g., Nd, Cs, Ra), which typically demand 20–200 L. This advantage in sample efficiency enables the generation of high-resolution datasets through cost-effective, large-scale sampling. By integrating REE signatures with hydrographic parameters, researchers can systematically quantify water mixing and nutrient contributions in the oligotrophic NPSG.

In this study, we aim to identify possible horizontal and vertical water sources in the upper southwestern NPSG. The water composition and nutrient flux subject to warm and/or cold eddies in three seasons (spring, summer, and winter) are further quantified by applying potential temperature, salinity, and REEs as tracers, and the modified optimum multiparameter analysis. In addition, the biological process and scavenging effect of REEs are discussed.

Survey and sampling: Samples from the southwestern NPSG were collected by R/V *TAN KAH KEE* during three GEOTRACES cruises (GP09 cruise from 27th April to 11th June 2019, GPpr15-summer cruise during 5th July to 17th August 2020, and GPpr15-winter cruise in 10th to 25th January 2021). Seawater for REEs was sampled from 12 L Niskin bottles with conductivity, temperature, and depth sensors (CTD, Sea-Bird 911 plus) and filtered through Pall AcroPak 1000 capsule (0.45 μm) filters. The filtrate for REEs analysis was acidified with 6 M ultra-pure hydrochloric acid (Optima grade, Fisher Chemical) to pH ≤ 2. All operations were carried out in a clean container. Seawater samples for nutrients (NO_x, PO_4, SiO_2) were filtered and frozen at −20°C and analyzed using a Four-channel Continuous Flow Technicon AA3 Auto-Analyzer (Bran-Lube GmbH) in the onshore laboratory (Du et al., unpubl.). The nutrient analysis followed the methodology described by Du et al. (2017) and Yuan et al. (2023). The analytical precision was 0.9% for NO_3^-, 0.6% for DIP, and 10.4% for NO_2^-. The alkalinity was measured by Gran titration (Cai et al. 2010) using an Apollo ALK2 Alkalinity Titrator, with a variation of ≤ 0.1% between three measurements. Details about sampling and measurement of alkalinity and nutrients can be found in Cai and Zhou (2019).

Seawater (100–150 mL) for REEs was pre-concentrated using NOBIAS-chelated PA-1® resin (Hatje et al. 2014). The eluent (2 mL 1 M nitric acid [HNO_3]) was determined by an inductively coupled plasma-mass spectrometer (ICP-MS, Thermo iCAP Q). The relative standard deviations (1σ RSD) of mean REE concentrations determined by replicate analysis of Pacific surface water ($n = 4$) were less than 5%. The normalized Ce anomaly $(Ce/Ce^*)_N$ was calculated as $(Ce/Ce^*)_N = (Ce)_N \times (Nd)_N/(Pr)_N^2$, where "N" refers to the Post-Archean Australian Shale (PAAS) (Taylor and McLennan 1985) normalization. $(HREE/LREE)_N$ was calculated by PAAS-normalized heavy REEs (Ho, Er, Tm, Yb) and light REEs (Pr, Nd). Data quality was confirmed by internationally conducted intercalibration between the laboratories of the Ocean University of China and the University of Southern Mississippi and confirmed by comparison with published GEOTRACES data (Behrens et al. 2018). The detailed methodology and intercalibration results were reported by Cao et al. (2024, 2025).

Modified optimum multiparameter analysis based on iterative REEs: To quantify the water fractions originating from different sources, eight REEs (Pr, Nd, Tb, Dy, Ho, Er, Tm, Yb) were used as additional tracers alongside potential temperature and salinity. Concentrations of La, Ce, Sm, Eu, and Gd were excluded because they are susceptible to the influence of non-conservative factors; La and Gd are prone to anthropogenic interference, exhibiting positive anomalies (Lim et al. 2023; Guan et al. 2022), while Ce and Eu are influenced by redox processes (Tanaka et al. 1990); Sm is affected by microbial activities, such as iron-manganese oxide reduction. Six water sources, including two vertical and four horizontal sources, were identified as end members and were featured in the discussion content. In this study, assuming that the water in the southwestern NPSG is in a steady state, Optimum Multiparameter (OMP) analysis was carried out following Che and Zhang et al. (2018) and Singh et al. (2012) and modified while employing the equations below:

$$\sum_{i=1}^{6} f_i = 1 + R_0 \quad (1)$$

$$\sum_{i=1}^{6} f_i \times \theta'_i = \theta'_{\text{sample}} + R_\theta \quad (2)$$

$$\sum_{i=1}^{6} f_i \times S'_i = S'_{\text{sample}} + R_S \quad (3)$$

$$\sum_{i=1}^{6} f_i \times [\text{REEs}]'_i = [\text{REEs}]'_{\text{sample}} + R_{\text{REEs}} \quad (4)$$

where "R" is the residual of the fit and "f" is the fraction of water sources. The subscript "sample" signifies the parameters of measured samples. θ', S', and $[\text{REEs}]'$ stand for the weighting-normalized potential temperature, salinity, and REE concentration, respectively. The weighting factors for θ and S and the REE concentration were estimated as 10 and 1, respectively, following the methodology outlined by Tomczak and Large (1989).

Because REEs are subject to non-conservative behavior in seawater (i.e., due to scavenging by particles), the $[\text{REEs}]'_{\text{sample}}$ in Eq. 4 has been influenced by more than just mixing so that the calculated water fractions could show deviation. Therefore, in order to remove the influence of scavenging, we refined Eq. 4 by replacing the measured REE concentrations in samples ($[\text{REEs}]'_{\text{sample}}$) with their calculated values ($\sum_{i=1}^{6} f_i[\text{REEs}]_i$) after the initial quantification, while holding potential temperature and salinity constant. As shown in Supporting Information Fig. S1, the modified vertical profiles of LREEs and HREEs with a weakened scavenging effect show a similar distribution. The modified OMP analysis was conducted again to get more accurate fractions based on Eqs. 1–3 and modified Eq. 4. This step was iterated several times until the calculated REE concentration remain constant, although the modifications were mainly generated in the first iteration. Details of the iterative process are given in Supporting Information Text S1. After the above modification, REE concentrations can be regarded as quasi-conservative tracers, since the influence of scavenging has been removed. The scavenging contribution can be quantified by

$$\alpha = \left([\text{REEs}]_{\text{sample}} - \sum_{i=1}^{6} f_i \times [\text{REEs}]_i \right) / \sum_{i=1}^{6} f_i \times [\text{REEs}]_i \quad (5)$$

where $[\text{REEs}]_{\text{sample}}$ is the measured concentration of the samples' REEs. Positive and negative values represent addition and scavenging, respectively.

Based on the quantified fractions of six water sources, the influence of biological processes on water components can be further calculated by

$$\Delta X = X_{\text{sample}} - \sum_{i=1}^{6} f_i \times X_i \quad (6)$$

where ΔX, such as ΔNutrient, represents the material consumption/production.

Results

Hydrography in the southwestern North Pacific Subtropical Gyre

The study area is located in the southwestern NPSG, primarily in the region of 11–21°N and 120–155°E, with the western stations being in close proximity to the Philippine Islands. The sea surface height (SSH) observations during sampling periods (Fig. 1) roughly reveal the widespread occurrence of warm (SSH > 1 m) and cold (SSH < 0.8 m) eddies in the northern region (> 12°N). Several cold eddies can also be identified in the southern region, although the SSH is lower than that of the northern region due to the influence of upwelling/downwelling near the Equatorial region (Dugdale and Wilkerson 1998; Johnson et al. 2001). In particular, the warm and cold eddies can be observed at stations K2/K2b (northwestern region) and K13/K13a (southwestern region, Mindanao Eddy, Chen et al. 2015), respectively.

Hydrographic and fluorescence data reveal eddy influences on water properties (Fig. 2). Warm eddy stations (e.g., K2, K3) show thermocline erosion from surface warm water sinking (0–300 m), while cold eddy stations exhibit rapid potential temperature shifts with depth, notably at K13 (26.1–18.3°C between 83 and 120 m). Cold water uplifting is also evident at Stations MR04 and K12a in summer and Station K13a in winter (Supporting Information Figs. S2, S3), with shallower summer uplift (50–150 m) vs. spring (50–300 m). Potential density contour deformations further confirm vertical water displacements. An important characteristic in the southwestern NPSG is that the fluorescence maximum can be observed in the bottom euphotic layer rather than in the shallower layers. Surface fluorescence remains weak due to nutrient limitation, increasing progressively with depth (Fig. 2e,f), suggesting vertical diffusion transports deeper nutrients into the bottom euphotic layer. Following Wu et al. (2021), we defined the bottom euphotic layer (89–219 m depth, station-dependent; Supporting Information Table S1) using 0.1% Photosynthetically Available Radiation (PAR) and 0.9% Usable Solar Radiation (USR) thresholds.

Vertical distribution of rare earth elements and Ce anomaly

Figure 3 displays vertical REE profiles, demonstrating higher REE concentrations in deeper layers than surface layers. Similar to the hydrographic patterns, stations near cold eddies (e.g., K13) exhibit elevated REE concentrations at 100–400 m depths compared to warm eddy stations (e.g., K2), though density-normalized plots (Fig. 3c,d) show minimal REE variability. An exception occurs at station K8 (eastern boundary, North Equatorial Current influence), displaying marginally lower heavy REE concentrations. $(\text{Ce/Ce}^*)_N$ and $(\text{HREE/LREE})_N$ (Fig. 3e,f) reveal consistent scavenging signatures. Shallow

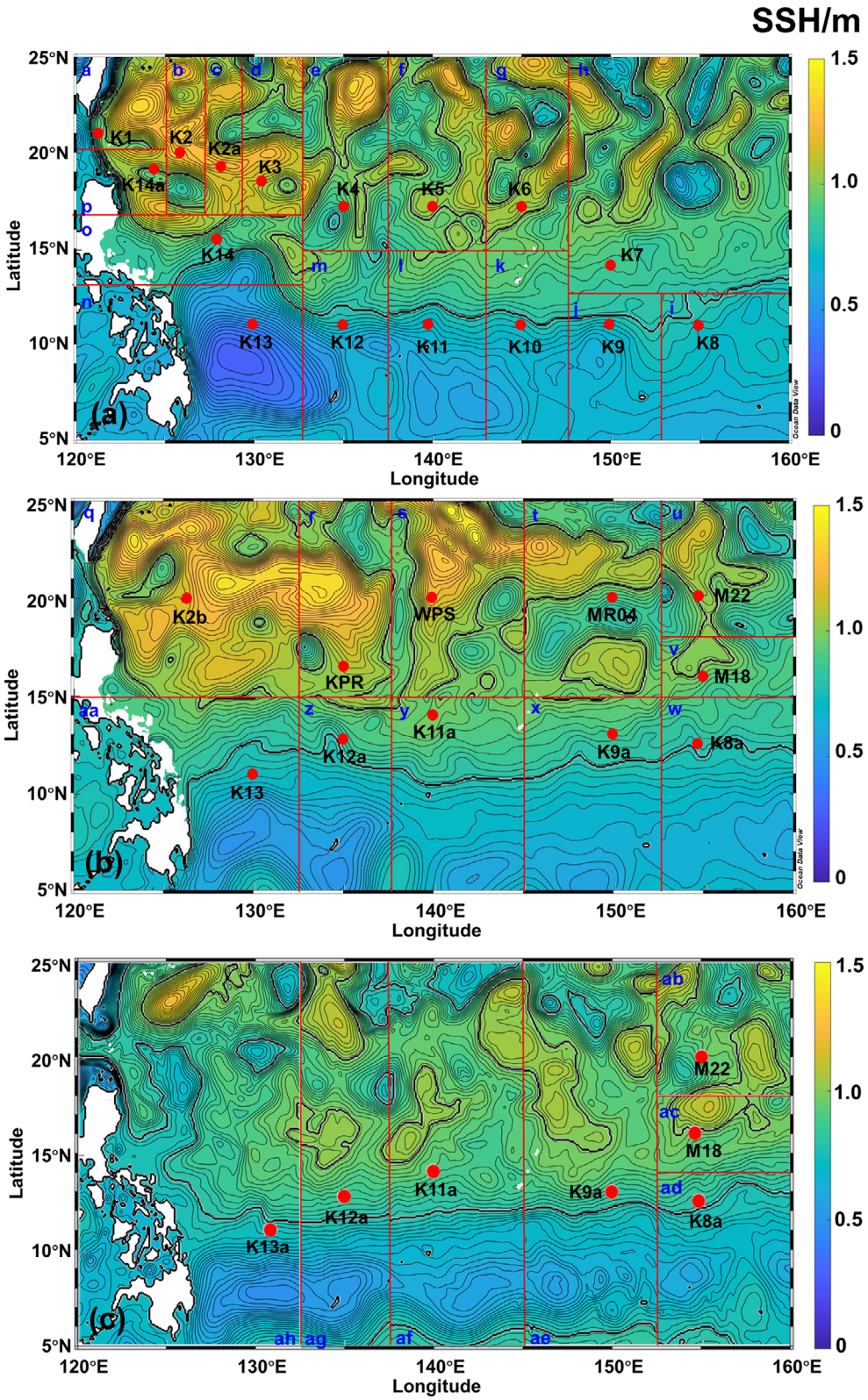

Fig. 1. Site maps with sea surface height (SSH) during the GP09 (**a**), GPpr15-summer (**b**), and GPpr15-winter (**c**) cruises. The SSH data shown at regions a to p (a), q to aa (b), and ab to ah (c) correspond to their respective sampling dates (April 27–May 1, 5, 3, 20, 21, 23, 25, 28, 31–June 2, 3, 5, 7, 8, and 10 in 2019; July 5, 11, 13, 19–August 1, 5, 7, 11, 13, 15, and 17 in 2020; January 10, 15, 17, 19, 21, 23, and 25 in 2021). Solid black lines show the contours of 0.8 m and 1.0 m. SSH data are referenced from Copernicus Marine Environment Monitoring Service.

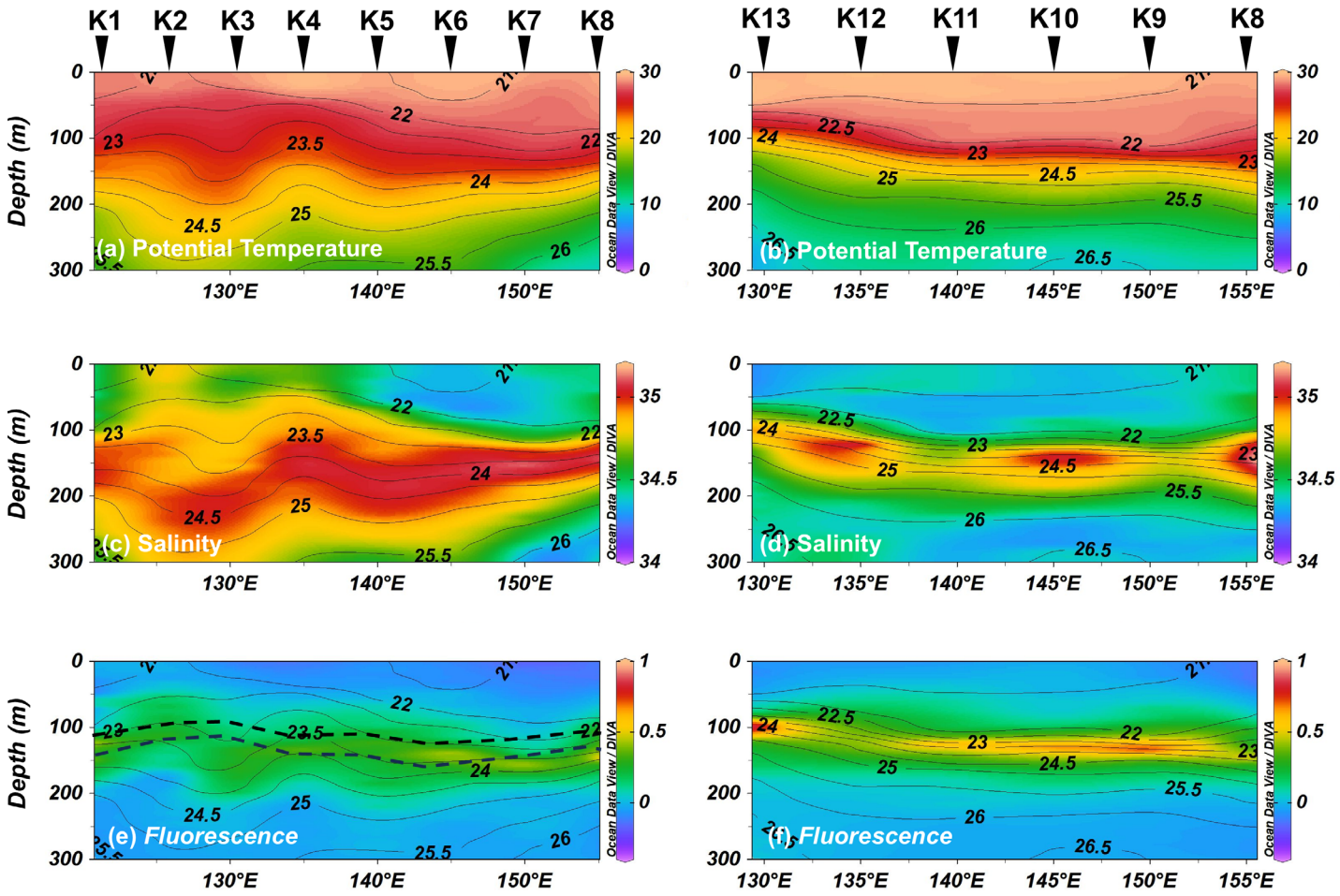

Fig. 2. Sections of potential temperature (**a**, **b**), salinity (**c**, **d**), and fluorescence (**e**, **f**) in spring contoured by potential density anomaly. Two black dashed lines in (e, f) represent the layer with 0.1% Photosynthetically Available Radiation (PAR) and 0.9% Usable Solar Radiation (USR), respectively.

layers (0–200 m), particularly the euphotic zone, show pronounced Ce anomalies (0.3–0.5 vs. deep layer 0.1), potentially linked to sunlight-inhibited microbial oxidation and scavenging (Moffett 1990). Notably, our Ce anomalies exceed those from high-productivity regions like the Sea of Japan and Southern Ocean, where primary productivity is high and scavenging by particles is more significant (Supporting Information Fig. S4). Moreover, $(HREE/LREE)_N$ in the shallow layers (0–100 m) is low and increases significantly from 100 m to 200 m, where enhanced biological processing can be observed by higher fluorescence. These results suggest that although REEs were reported to be not completely conservative due to scavenging (Byrne and Kim 1990), the effect is relatively weak in the southwestern NPSG.

Discussion

To evaluate the water mixing and nutrient supply in the shallow southwestern NPSG, four horizontal and two vertical water sources were identified. Using modified OMP analysis with REE-hydrographic tracers, we quantified source contributions, validating results through measured vs. calculated alkalinity comparisons. Moreover, the study examined the influence of various factors on REEs, such as scavenging, shedding light on the processes affecting the REE distribution. Finally, through quantifying the water contribution from each water source, nutrient fluxes were estimated at stations during three seasons: spring, summer, and winter.

Identifying horizontal and vertical water sources

Six water sources contributing to the southwestern NPSG waters were identified. Four horizontal sources were used based on the current distribution, namely the North Equatorial Current-derived water (NEC-derived), Equator-derived water (EQ-derived), Coast-derived water (CW-derived), and northern NPSG-derived water (nNPSG-derived) (Fig. 4a). Horizontal source data represent mean regional characteristics in different directions (e.g., ALOHA station for eastern NEC waters), with selection based on density matching (isopycnal

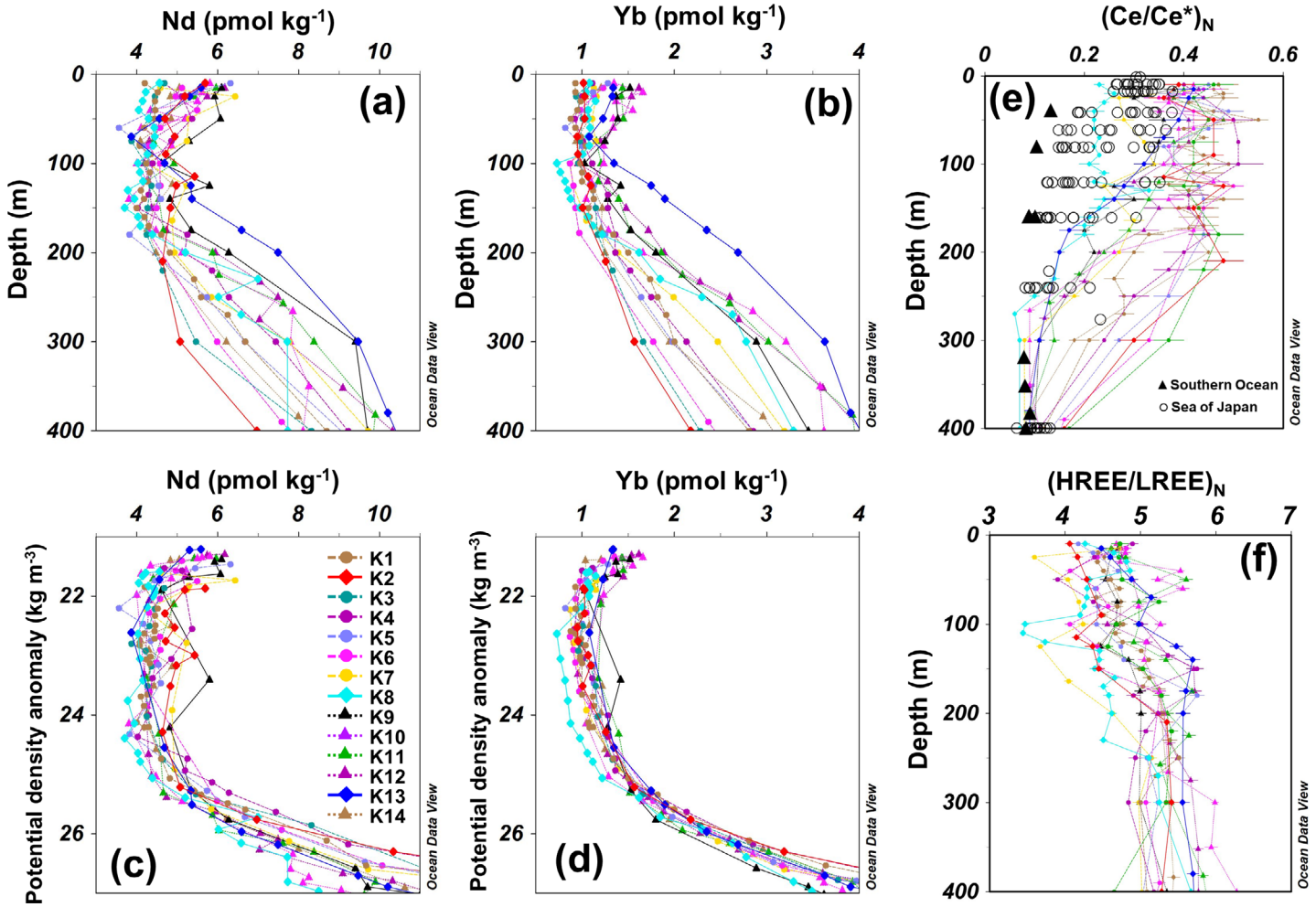

Fig. 3. Vertical profiles of REEs, $(Ce/Ce^*)_N$, and $(HREE/LREE)_N$ with depth and density as vertical axes.

transport) between source and study area samples. CW-derived data originated from the Sulu Sea (Nozaki et al. 1999; Takeda et al. 2007), due to Philippine coastal data scarcity, with exchange pathways via the Semirara Sea (Metzger and Hurlburt 1996; Hu et al. 2000). Despite potential systematic bias in CW quantification, its minor contributions (Fig. 5; Supporting Information Fig. S7) minimally affect overall calculations. In this study, the influence of South China Sea water outflow (Chen and Wang 1998) was determined to be insignificant by comparing hydrographic data from Stations K1–K4, K14, and adjacent South China Sea water (Supporting Information Fig. S5). In addition, to further quantify the contribution of vertical water mixing, two additional water sources were defined: surface water (SW) at $\sigma_\theta < 22.0$ kg m^{-3} and deep water (DW) at $\sigma_\theta \sim 25.22$–26.50 kg m^{-3}. DW was defined by the influence of mesoscale eddies, extending to depths of approximately 300 m (Wilson 2021), where water properties remained constant during westward transport (Supporting Information Fig. S6).

Water sources were characterized using potential temperature, salinity, and REEs (*see* Supporting Information Table S2). Temperature/salinity differentiated water types (e.g., warm SW, low-salinity CW; Fig. 4b), while distinct REE signatures (concentration ratios and fractionation patterns; Fig. 4c) enhanced source discrimination. As an example, if we focus on the Er_N/Yb_N and Er_N/Nd_N (Fig. 4d,e), the sample at station K13 with a depth of 125 m was formed by the mixing of six water sources. Critically, this target sample cannot be constructed solely from the four horizontal sources shown in Fig. 4d. The necessity of the DW source to form this sample indicates the presence of vertical mixing processes.

Quantifying horizontal and vertical water mixing

Water contributions from six sources across seasons in the southwestern NPSG were quantified via modified OMP analysis. NEC-derived dominated in three seasons (61% ± 20% average), though shallow layers of summer showed reduced contributions from EQ-derived intrusion. CW-derived partially

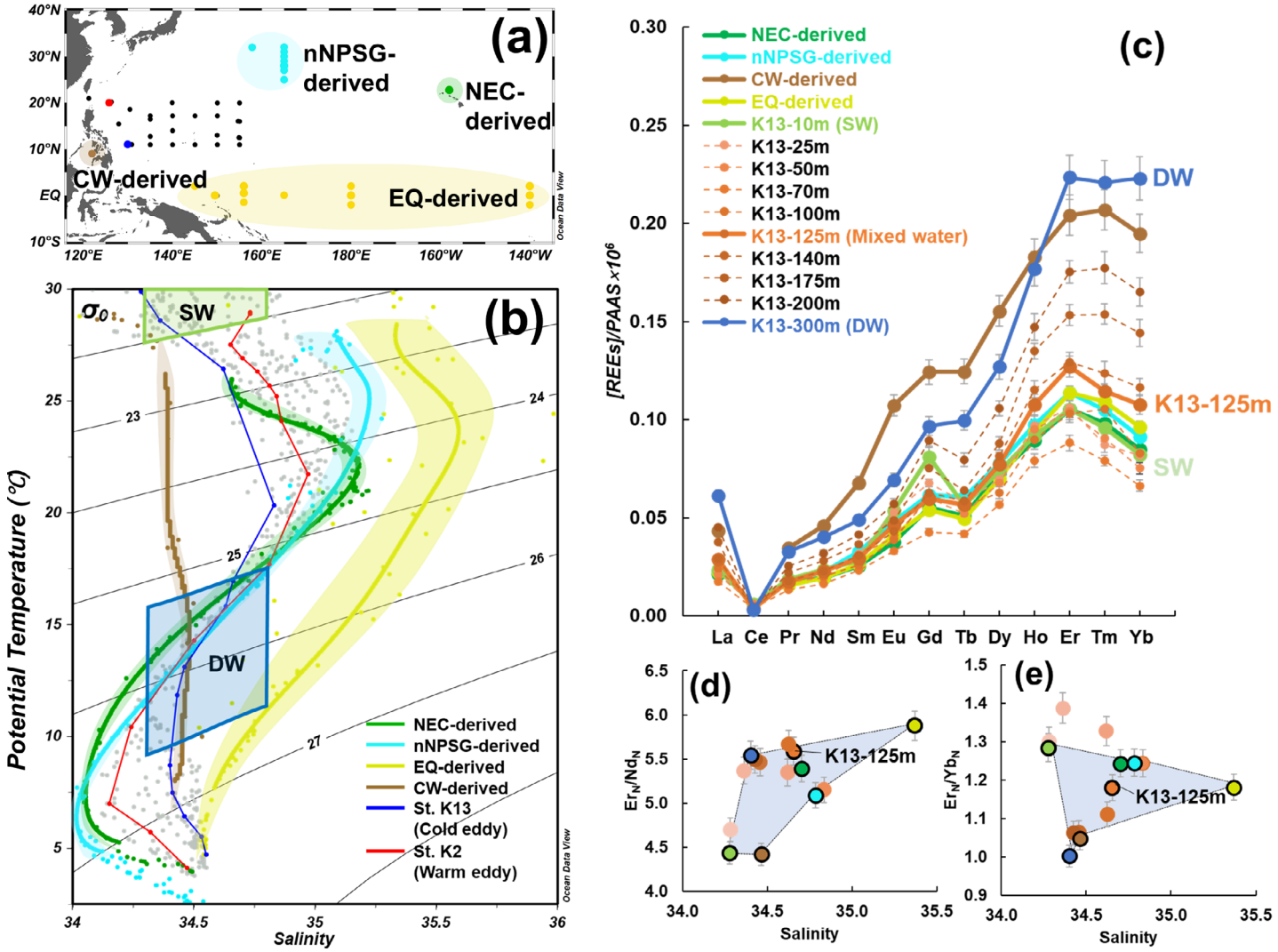

Fig. 4. Distribution of stations (**a**), T-S diagram (**b**) and REE patterns (**c**). SW (Salinity: 34.30–34.80, σ_θ: <22.0 kg m^{-3}) and DW (Salinity: 34.32–34.81, σ_θ: 25.22–26.50 kg m^{-3}) in (b) were identified in the shallow green and blue areas, respectively. Shaded areas in (b) show data variation of four horizontal water sources and the curves in shaded areas represent mean data. The REE pattern of each water source in (c) is shown at a density similar to that of K13-125 m (25.28 kg m^{-3}). (**d**, **e**): Colored dots with black circles show the water sources; subscript "N" represents Post-Archean Australian Shale normalization.

contributes to the southwestern NPSG but in an inconsistent way. EQ-derived and nNPSG-derived waters exhibit inverse density distributions, with temperature-driven stratification: warmer EQ-derived waters dominate shallower layers (< 23.5 kg·m^{-3}), while colder nNPSG-derived waters sink deeper (150–250 m). This confirms the subtropical mode water intrusion reported by Huang et al. (2021) and Zhu et al. (2023). Warm eddy (e.g., Stations K2, K3; 50–120 m) elevated SW (Station K2: 29% ± 12%; K3: 14% ± 10%) vs. adjacent stations (Station K1: 11% ± 7%; K4: 12% ± 3%). Cold eddy (e.g., Stations K12, K13; 125–140 m) suppressed SW (Station K12: 11% ± 6%; K13: 4% ± 0%) vs. adjacent stations (Station K11: 26% ± 2%; K14: 11% ± 7%). Please *see* more details in Supporting Information Text S2, Supporting Information Fig. S7, and Supporting Information Tables S3–S5.

To validate calculations, measured and modeled alkalinities were compared (Supporting Information Fig. S8), leveraging alkalinity's conservative nature in the upper ocean. Calculated values show < 1.0% (mostly < 0.5%) deviation from measurements. Considering the measurement precision (0.1%) of alkalinity data and the uncertainties of parameters used in the OMP analysis, the calculation results can provide relatively reasonable information.

Optimum Multiparameter analysis uncertainties primarily stem from REE end-member selection and measurement errors

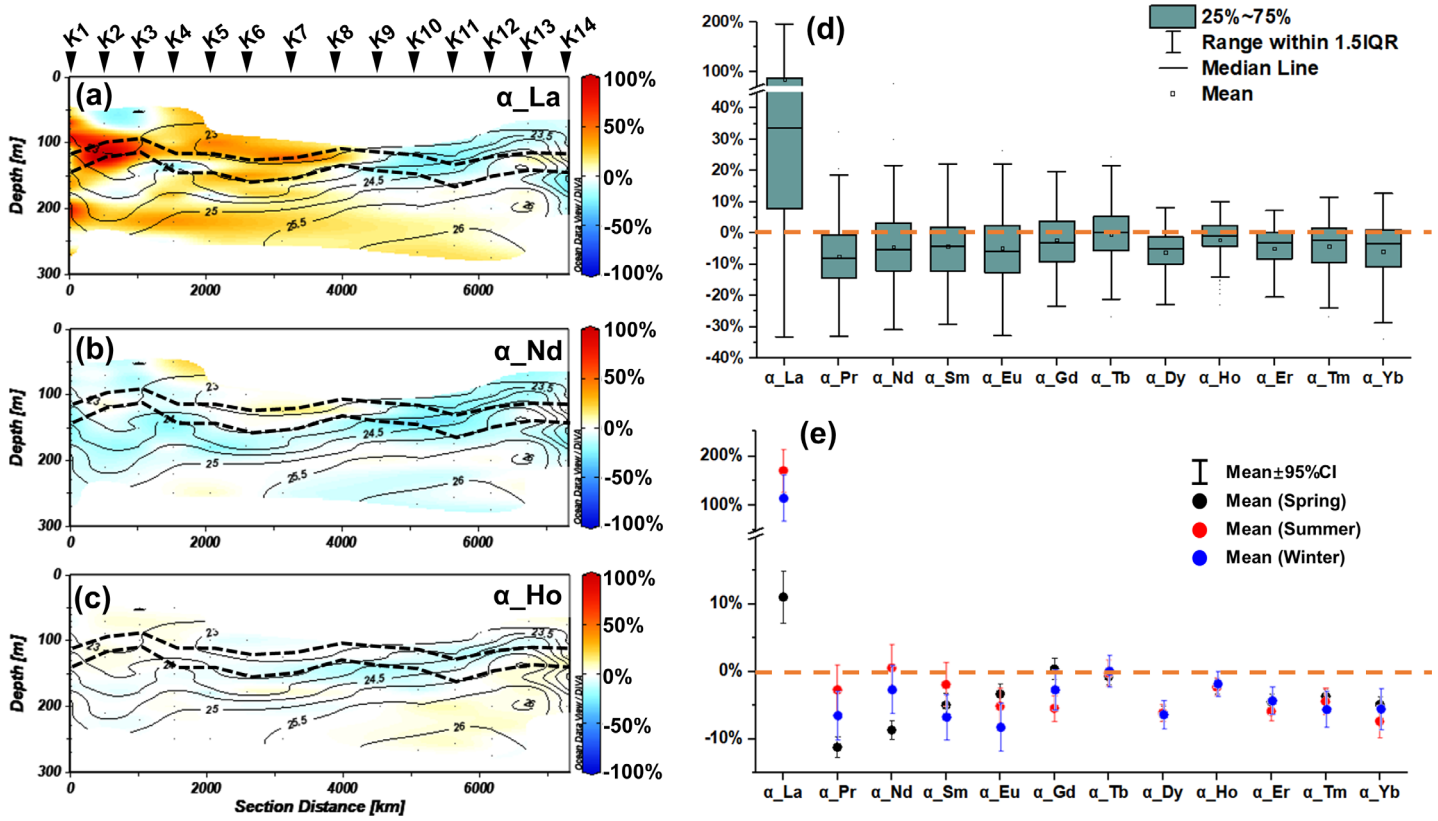

Fig. 5. Section maps of α_La (**a**), α_Nd (**b**), and α_Ho (**c**) in spring contoured by potential density anomaly, box plot (**d**) of all α_REE data ($n = 214$), and interval plot (**e**) in three seasons. Dashed lines in (a-c) represent the bottom euphotic layer.

(REE RSD < 5%). Recalculations with ± 5% REE adjustments (Supporting Information Table S6) yielded mean OMP analysis deviations < 3% (euphotic-zone samples: < 2%). Recombined source calculations (Supporting Information Tables S7, S8) produced mean deviations < 4%. Fractions of samples using different combinations of chemical tracers showed similar results (correlation coefficient $r = 0.96 \pm 0.07$, $p < 0.0001$, $n = 30$). Please *see* Supporting Information Text S3, S4, Supporting Information Fig. S9, and Supporting Information Table S9 for details. Considering the divergence of the contribution fractions (> 10%) of the individual water sources, the OMP analysis results do not show significant uncertainty.

Scavenging effect by particles from biological process on the rare earth element distribution

REE distributions exhibit non-conservative behavior due to particle scavenging linked to biological activity, observed both locally and along horizontal transport pathways. Fluorescence maxima, elevated nutrient supply, and transmission reductions co-occur at 100–150 m depths, with scavenging intensity strongly correlating with fluorescence ($r = -0.64$, $p < 0.00001$) (Supporting Information Text S5; Supporting Information Fig. S10e). Net REE removal (excluding La, Fig. 5) is quantified, showing preferential adsorption of light REEs (e.g., Minimum Nd: −31%) over heavy REEs (Minimum Ho: −19%), with minimal α-values in the euphotic zone where biological activity peaks. α_Ce was not provided in this study because the Ce data of six water sources show large variations in vertical profiles, and α_Ce is difficult to quantify. La anomalies, likely coal/anthropogenic in origin (Song et al. 2017), are concentrated in northern sections, transported eastward via the Subtropical Countercurrent (~ 20°N; Qiu et al. 2014). Despite detectable scavenging, its impact remains limited in the southwestern NPSG due to nutrient depletion and weak biological activity. Within the mean ± 95% confidence interval (CI), all REEs (except La) show < 15% scavenging influence (Fig. 5e).

Biological processes affecting REE distribution were identified based on the water-mixing fractions of six water sources. This study estimated the consumption/production of dissolved inorganic nitrogen (ΔDIN) and phosphate (ΔDIP) using Eq. 6. Negative values in shallow layers indicate nutrient consumption, while positive values in deep layers signify nutrient release. The DIN shows a good linear relationship with DIP, with the slope at 14.06 ± 0.17. ΔDIN–ΔDIP correlations reveal dual trends: bulk samples follow a slope of

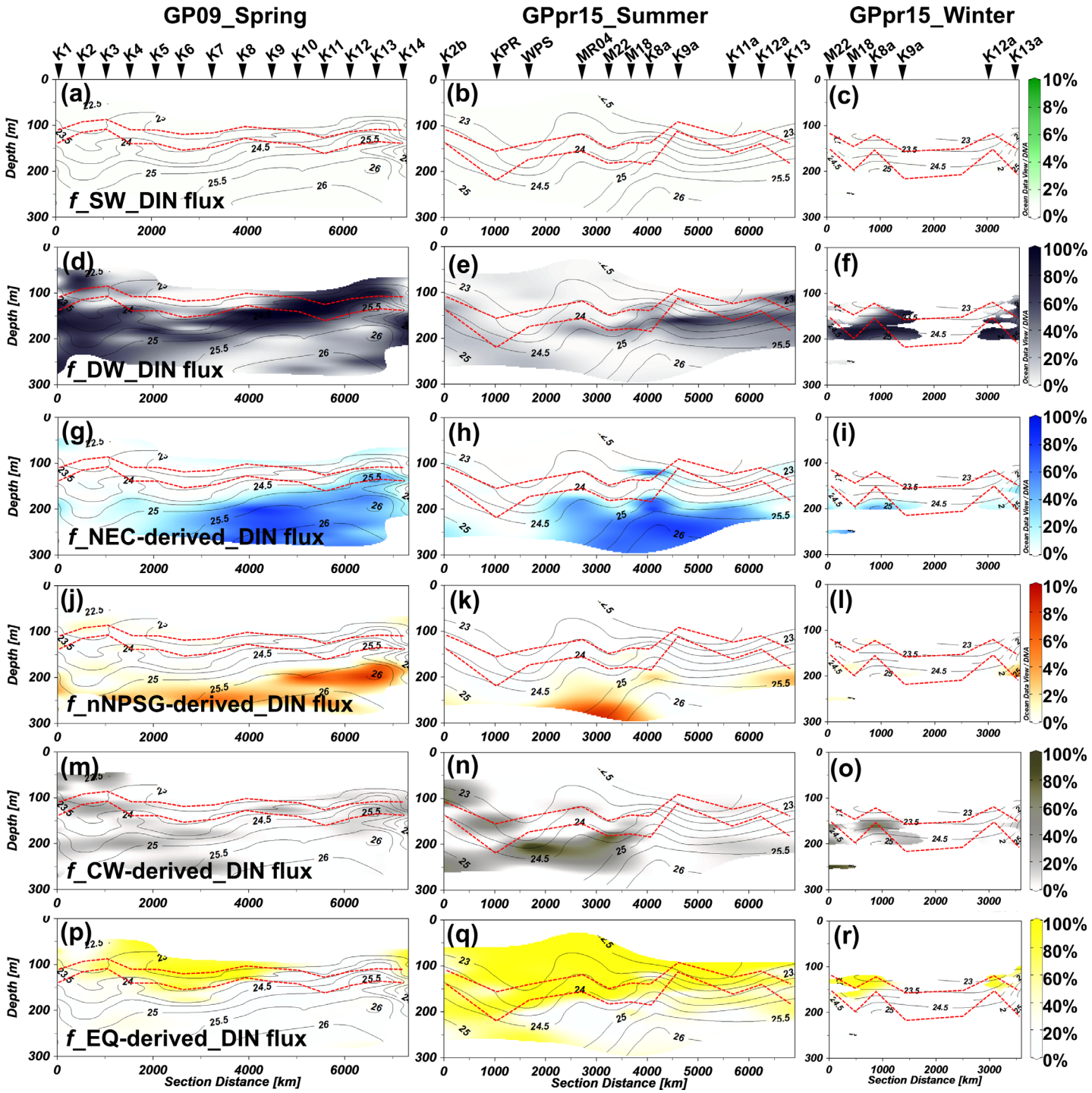

Fig. 6. DIN contribution of SW (**a**–**c**), DW (**d**–**f**), NEC-derived (**g**–**i**), nNPSG-derived (**j**–**l**), CW-derived (**m**–**o**), and EQ-derived (**p**–**r**) contoured by potential density anomaly. The color bars show the contribution fractions of DIN from six sources. Red dashed lines represent the layers with 0.1% Photosynthetically Available Radiation (PAR) and 0.9% Usable Solar Radiation (USR).

11.47 ± 0.31, while upper 140 m samples (ΔDIP: −0.4–0 μM) display a lower slope (10.99 ± 0.28) and intercept (0.76 ± 0.07). Please *see* more details in Supporting Information Text S6 and Supporting Information Fig. S11.

Estimating horizontal and vertical nutrient supply in the southwestern North Pacific Subtropical Gyre

Horizontal and vertical nutrient supply was quantified using water source fractions and concentrations via:

$$\text{Nutrient}\% = f_i \times [\text{Nutrient}]_i / \left(\sum_{i=1}^{6} f_i \times [\text{Nutrient}]_i \right)$$

where $[\text{Nutrient}]_i$ represents the nutrient concentration of each water source. The results are summarized in Fig. 6 and Supporting Information Tables S11–S13.

Horizontal mixing: NEC-derived, nNPSG-derived, EQ-derived, and CW-derived contribute 10% ± 19%, 0% ± 1%, 7% ± 15%, 51% ± 37% of DIN supply at a depth of ≤ 200 m, respectively. (1) NEC-derived fractions are high at a depth of 200–300 m (mean: 38% ± 26%, spring: 39% ± 26%, summer: 41% ± 32%, winter: 27% ± 15%) but low in shallow layers. (2) Contributions decline westward (e.g., 200 m in spring; Stations K8–K14: 85% ± 3%, 74% ± 2%, 69% ± 2%, 43% ± 3%, 47% ± 3%, 35% ± 4%, and 20% ± 1%), reflecting mixing during NEC westward transport. (3) nNPSG-derived (0%–9%) and EQ-derived (45% ± 36%) preferentially influence > 200 m and < 150 m layers, respectively. (4) CW-derived only show high nutrient contribution in specific water parcels.

Vertical mixing: The nutrient contribution of vertical mixing at a depth of ≤ 200 m is not negligible (DW: 31% ± 32%, SW: 0% ± 0%), contrasting prior models emphasizing horizontal transport (Letscher et al. 2016). (1) The nutrient contribution of DW in spring (44% ± 35%) and winter (44% ± 32%) is higher than that in summer (15% ± 20%) due to stratification (Fujiki et al. 2016). (2) Southern regions show higher DW-driven DIN (54% ± 33%, Stations K9–K13) than northern areas (33% ± 31%, Stations K2–K7), consistent with equatorial upwelling. (3) SW makes no contribution (surface nutrient concentration ≈ 0 μM).

Total horizontal (four sources) and vertical (SW and DW) nutrient supplies in the bottom euphotic layer were calculated as $\text{Nutrient supply}_i = \sum f_i \times [\text{Nutrient}]_i$ (mmol m^{-3}; mixing periods excluded due to spatiotemporal variability; Fig. 7). Total supplies were higher at southern stations (K9–K13, spring: 2.3–7.6 mmol m^{-3}) than at northern stations (K2–K7: 1.3–2.2 mmol m^{-3}), driven primarily by cold eddies and upwelling. These processes uplifted nutrient-rich waters, enhancing both vertical and horizontal DIN supplies. For instance, at 300 m depth, Station K13 (density 26.71 kg m^{-3}) exhibited elevated DIN concentrations (30.35 μM) compared to Station K2 (25.22 kg m^{-3}, 4.64 μM), resulting in vertical DIN supplies of 2.3–5.1 mmol m^{-3} at K13, far exceeding those at K2. In contrast, non-eddy stations (e.g., Stations K7 in spring, M18 in summer) exhibited minimal vertical (0–0.1 mmol m^{-3}) but notable horizontal DIN supply (1.4–2.0 mmol m^{-3}). Despite the elevated southern DIN supplies, the ΔDIN remains

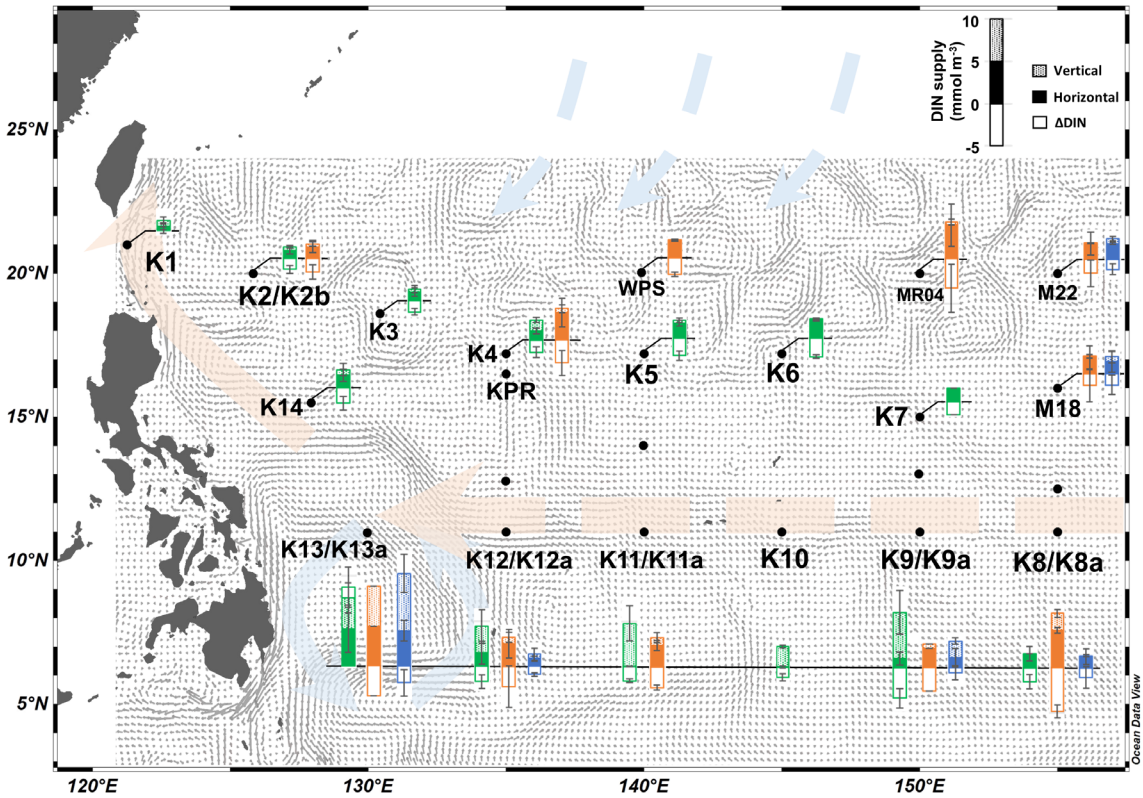

Fig. 7. DIN supply in the bottom euphotic layer in spring (green), summer (orange), and winter (blue). The negative ΔDIN values represent nutrient consumption. The arrows indicate the current distribution. The small arrows show the current velocity on 1st June 2019 (current velocity data are from Copernicus Marine Environment Monitoring Service). The black baselines in each histogram show 0 mmol m^{-3} DIN supply.

Table 1. DIN flux in the bottom euphotic layer of this study and in previous studies.

Sources	DIN flux/mmol N m^{-2} d^{-1}	Depth-integrated N_2 fixation (upper 100-m)/mmol N m^{-2} d^{-1}	POC flux/mg C m^{-2} d^{-1}
Vertical flux near warm eddy	0.10–0.76 (0.45 ± 0.11)*	0.48 ± 0.09†	8.0–60
Vertical flux near cold eddy	0.21–2.13 (1.20 ± 0.36)*	0.013 ± 0.011†	15.9–169
Vertical flux without eddy	0.066–0.53 (0.33 ± 0.06)*	0.18 ± 0.18†	5.2–42
Mean vertical flux in this study	0.083–0.64		
Mean vertical flux in the NPSG by models‡	10^{-2} to 10^{-1}		
Vertical flux in the subarctic and subtropical area without eddy§	10^{-3} to 10^{-2}		
Observed POC fluxes in the Northwest Pacific‖			83–194 (warm eddy) 26–35 (no eddy)

*DIN fluxes in brackets show average values.
†Data are from Wen et al. 2022.
‡Data are from Mouriño-Carballido et al. 2021.
§Data are from Kaneko et al. 2021.
‖Data are from Shih et al. 2015.

low, likely due to Fe-limitation (Wen et al. 2022), which limits biological activity in this region.

In this study, different eddies can be a key influencing factor of nutrient supply in the southwestern NPSG. In order to evaluate the influence of different eddies, stations in the northern region were classified into three groups based on the SSH (Fig. 1): Group I (stations influenced by warm eddies: K2, K3, K5, K5 in spring; K2b, KPR, WPS, M22 in summer; M18 in winter), Group II (stations influenced by cold eddies: K4 in spring; MR04 in summer), Group III (stations without eddy: K7 in spring; M18 in summer; M22 in winter). Stations near the Luzon Strait (K1) and those < 12°N were excluded due to topographic mixing and equatorial upwelling interference, respectively. Vertical DIN fluxes were calculated by $f_{DW} \times [DIN]_{DW} \times (300\ m - [\text{depth of bottom euphotic layer}])/T$, where $[DIN]_{DW}$ and T represent the DIN concentration of DW and the residence time, respectively. The residence time T was estimated from eddy lifetimes (11 weeks–430 d with an average of 3.5 months, Wilson 2021), assuming a relatively steady state during the eddy mixing process (*see* details in Supporting Information Text S7).

The mean vertical DIN fluxes for warm eddies, cold eddies, and non-eddy stations were 0.45 ± 0.11 (0.10–0.76), 1.20 ± 0.36 (0.21–2.13), and 0.33 ± 0.06 (0.066–0.53) mmol m^{-2} d^{-1}, respectively (Table 1). These values exceed model estimates for the broader NPSG (10^{-2}–10^{-1} mmol m^{-2} d^{-1}; Mouriño-Carballido et al. 2021) and other subtropical areas (10^{-3}–10^{-2} mmol m^{-2} d^{-1}, Kaneko et al. 2021). This can be explained by the mean eddy frequency in this area (reported as 0.10–0.20, Yang et al. 2013), since eddies cannot be present at all times to enhance the nutrient supply. Moreover, in Fig. 1, the areas with warm (SSH > 1.0 m), cold (SSH < 0.8 m), and no eddies were roughly estimated at 31.0%, 4.36%, and 64.6% of the eddy region (123–160°E, 12–25°N); note that the eddy region was only identified in the northern part (> 12°N) since the southern stations can be influenced both by eddy and upwelling. Regionally, the mean vertical flux (0.083–0.64 mmol m^{-2} d^{-1}) aligned with model predictions. Previously, nitrogen fixation was considered as another key nitrogen source in the oligotrophic NPSG (Fong et al. 2008; Karl et al. 1997), but our results suggest that cold eddies could enhance vertical DIN supply by 20–100 times compared to nitrogen fixation rates (Wen et al. 2022), whereas warm/non-eddy zones showed comparable contributions from both processes.

Elevated vertical DIN supply could enhance CO_2 adsorption, while CO_2 uptake is also constrained by factors such as CO_2 fugacity (Pan et al. 2015). Using the Redfield ratio (C : N = 106 : 16), the particulate organic carbon (POC) export flux derived from vertical nutrient supply is roughly estimated at 5–169 mg C m^{-2} d^{-1}, which is slightly lower than the fluxes observed by sediment traps (83–194 mg C m^{-2} d^{-1}) at a station near a warm eddy (Shih et al. 2015). These POC fluxes are much higher than those at oligotrophic reference waters (26–35 mg C m^{-2} d^{-1}, Shih et al. 2015), where eddy-driven nutrient uplift is minimal. Considering the widespread presence of eddies in the global ocean, further studies on their contribution to carbon circulation in the ocean can be expected. In particular, as oceanic primary production could decline significantly due to global warming (Yuval and Kaspi 2020; Couespel et al. 2021), mesoscale eddies could play a more important role in adjusting the material balance and ecosystem in global oceans.

Author Contributions

Siteng J. Zhu contributed to writing – original draft preparation. Jing Zhang and Qian Liu worked for conceptualization, supervision, funding acquisition. Qian Liu, Alan M. Shiller, and

Zhimian Cao contributed to investigation and resources. Jing Zhang, Qian Liu, Alan M. Shiller, Chuanjun Du, Xianghui Guo, Yihua Cai, and Xin Liu worked for writing – review and editing.

Acknowledgments

We thank the captain and all crew members and scientists on the R/V *TAN KAH KEE* for help with the observations and samplings. We thank Wanyang He, Wenkai Guan for the REE sample collection. We thank Axiang Cao, Zhensong Liu, and Melissa Gilbert for the REE sample measurement, and Lifang Wang for the nutrient sample collection and analysis. This work was supported by the National Key Research and Developmental Program of China (Grant 2023YFF0805001), the JSPS KAKENHI (Grant JP24K03061, JP22H05206 and JP20H04319), and the US NSF (Grant OCE-1925503). The International GEOTRACES Programme is possible in part thanks to the support from the U.S. National Science Foundation (Grant OCE-2513154) to the Scientific Committee on Oceanic Research (SCOR).

Conflicts of Interest

None declared.

Data Availability Statement

SSH data in this study were referenced from Copernicus Marine Environment Monitoring Service (GLOBAL_ANALYSIS_FORECAST_PHY_001_024, https://doi.org/10.48670/moi-00016 and GLOBAL_MULTIYEAR_PHY_001_030, https://doi.org/10.48670/moi-00021). JMA data in this study were referenced from Japan Meteorological Agency (https://www.data.jma.go.jp/kaiyou/db/vessel_obs/data-report/html/ship/ship.php). Datasets used in the study are available at Dryad: (https://doi.org/10.5061/dryad.qrfj6q5qf).

References

Alibo, D. S., and Y. Nozaki. 1999. "Rare Earth Elements in Seawater: Particle Association, Shale-Normalization, and Ce Oxidation." *Geochimica et Cosmochimica Acta* 63: 363–372. https://doi.org/10.1016/S0016-7037(98)00279-8.

Barone, B., M. J. Church, M. Dugenne, et al. 2022. "Biogeochemical Dynamics in Adjacent Mesoscale Eddies of Opposite Polarity." *Global Biogeochemical Cycles* 36: e2021GB007115. https://doi.org/10.1029/2021GB007115.

Behrens, M. K., J. Muratli, C. Pradoux, et al. 2016. "Rapid and Precise Analysis of Rare Earth Elements in Small Volumes of Seawater—Method and Intercomparison." *Marine Chemistry* 186: 110–120. https://doi.org/10.1016/j.marchem.2016.08.006.

Behrens, M. K., K. Pahnke, R. Paffrath, B. Schnetger, and H.-J. Brumsack. 2018. "Rare Earth Element Distributions in the West Pacific: Trace Element Sources and Conservative vs. Non-Conservative Behavior." *Earth and Planetary Science Letters* 486: 166–177. https://doi.org/10.1016/j.epsl.2018.01.016.

Byrne, R. H., and K.-H. Kim. 1990. "Rare Earth Element Scavenging in Seawater." *Geochimica et Cosmochimica Acta* 54: 2645–2656. https://doi.org/10.1016/0016-7037(90)90002-3.

Cai, W.-J., X. Hu, W.-J. Huang, et al. 2010. "Alkalinity Distribution in the Western North Atlantic Ocean Margins." *Journal of Geophysical Research: Oceans* 115: C08014. https://doi.org/10.1029/2009JC005482.

Cai, Y., and K. Zhou. 2019. "*4.1. Conventional CTD*." GEOTRACES-CHINA GP09 wNP Section Study Cruise Report 8 https://doi.org/10.1080/23802359.2019.1700194.

Cao, A., Q. Liu, J. Zhang, et al. 2025. "Spatiotemporal Variation of Dissolved Rare Earth Elements in the North Pacific Subtropical Gyre: Influence of Biogeochemical Cycling and Application in Tracing Deep Water." *Global and Planetary Change* 246: 104719. https://doi.org/10.1016/j.gloplacha.2025.104719.

Cao, A., Q. Liu, J. Zhang, et al. 2024. "Dissolved Rare Earth Elements in the North Pacific Subtropical Gyre: Lithogenic Sources and Water Mass Mixing Control." *Geochimica et Cosmochimica Acta* 372: 42–61. https://doi.org/10.1016/j.gca.2024.02.018.

Chelton, D. B., P. Gaube, M. G. Schlax, J. J. Early, and R. M. Samelson. 2011. "The Influence of Nonlinear Mesoscale Eddies on Near-Surface Oceanic Chlorophyll." *Science* 334: 328–332. https://doi.org/10.1126/science.1208897.

Chen, C.-T. A., and S.-L. Wang. 1998. "Influence of Intermediate Water in the Western Okinawa Trough by the Outflow From the South China Sea." *Journal of Geophysical Research: Oceans* 103: 12683–12688. https://doi.org/10.1029/98JC00366.

Chen, F., J. Chen, G. Jia, et al. 2013. "Nitrate δ 15N and δ 18O Evidence for Active Biological Transformation in the Changjiang Estuary and the Adjacent East China Sea." *Acta Oceanologica Sinica* 32: 11–17. https://doi.org/10.1007/s13131-013-0294-4.

Chen, L., Y. Jia, and Q. Liu. 2015. "Mesoscale Eddies in the Mindanao Dome Region." *Journal of Oceanography* 71: 133–140. https://doi.org/10.1007/s10872-014-0255-3.

Chen, X., B. Qiu, S. Chen, and Y. Qi. 2021. "Period-Lengthening of the Mindanao Current Variability From the Long-Term Tide Gauge Sea Level Measurements." *Journal of Geophysical Research: Oceans* 126: e2020JC016932. https://doi.org/10.1029/2020JC016932.

Cheng, Y.-H., C.-R. Ho, Q. Zheng, and N.-J. Kuo. 2014. "Statistical Characteristics of Mesoscale Eddies in the North Pacific Derived From Satellite Altimetry." *Remote Sensing* 6: 5164–5183. https://doi.org/10.3390/rs6065164.

Chou, W.-C., D. D. Sheu, C. T. A. Chen, L.-S. Wen, Y. Yang, and C.-L. Wei. 2007. "Transport of the South China Sea Subsurface Water Outflow and its Influence on Carbon Chemistry of Kuroshio Waters off Southeastern Taiwan." *Journal of Geophysical Research: Oceans* 112: C12008. https://doi.org/10.1029/2007JC004087.

Couespel, D., M. Lévy, and L. Bopp. 2021. "Oceanic Primary Production Decline Halved in Eddy-Resolving Simulations

of Global Warming." *Biogeosciences* 18: 4321–4349. https://doi.org/10.5194/bg-18-4321-2021.

Du, C., Z. Liu, S.-J. Kao, and M. Dai. 2017. "Diapycnal Fluxes of Nutrients in an Oligotrophic Oceanic Regime: The South China Sea." *Geophysical Research Letters* 44: 11510–11518. https://doi.org/10.1002/2017GL074921.

Dugdale, R. C., and F. P. Wilkerson. 1998. "Silicate Regulation of New Production in the Equatorial Pacific Upwelling." *Nature* 391: 270–273. https://doi.org/10.1038/34630.

Falkowski, P. G., D. Ziemann, Z. Kolber, and P. K. Bienfang. 1991. "Role of Eddy Pumping in Enhancing Primary Production in the Ocean." *Nature* 352: 55–58. https://doi.org/10.1038/352055a0.

Fong, A. A., D. M. Karl, R. Lukas, R. M. Letelier, J. P. Zehr, and M. J. Church. 2008. "Nitrogen Fixation in an Anticyclonic Eddy in the Oligotrophic North Pacific Ocean." *ISME Journal* 2: 663–676. https://doi.org/10.1038/ismej.2008.22.

Fujiki, T., K. Sasaoka, K. Matsumoto, M. Wakita, and Y. Mino. 2016. "Seasonal Variability of Phytoplankton Community Structure in the Subtropical Western North Pacific." *Journal of Oceanography* 72: 343–358. https://doi.org/10.1007/s10872-015-0346-9.

Guan, W., H. He, and J. Zhang. 2022. "Sources and Fluxes of Rare Earth Elements in Wet Deposition at a Chinese Coastal City Downstream of the Asian Continental Outflow." *Atmospheric Environment* 269: 118843. https://doi.org/10.1016/j.atmosenv.2021.118843.

Hara, Y., H. Obata, T. Doi, et al. 2009. "Rare Earth Elements in Seawater During an Iron-Induced Phytoplankton Bloom of the Western Subarctic Pacific (SEEDS-II)." *Deep Sea Research Part II: Topical Studies in Oceanography* 56: 2839–2851. https://doi.org/10.1016/j.dsr2.2009.06.009.

Hatje, V., K. W. Bruland, and A. R. Flegal. 2014. "Determination of Rare Earth Elements After Pre-Concentration Using NOBIAS-Chelate PA-1®Resin: Method Development and Application in the San Francisco Bay Plume." *Marine Chemistry* 160: 34–41. https://doi.org/10.1016/j.marchem.2014.01.006.

Hu, J., H. Kawamura, H. Hong, and Y. Qi. 2000. "A Review on the Currents in the South China Sea: Seasonal Circulation, South China Sea Warm Current and Kuroshio Intrusion." *Journal of Oceanography* 56: 607–624. https://doi.org/10.1023/A:1011117531252.

Huang, W.-J., M.-T. Lee, K.-C. Huang, et al. 2021. "Radiocesium in the Taiwan Strait and the Kuroshio East of Taiwan From 2018 to 2019." *Scientific Reports* 11: 22467. https://doi.org/10.1038/s41598-021-01895-y.

Johnson, G. C., M. J. McPhaden, and E. Firing. 2001. "Equatorial Pacific Ocean Horizontal Velocity, Divergence, and Upwelling." *Journal of Physical Oceanography* 31: 839–849. https://doi.org/10.1175/1520-0485(2001)031<0839:EPOHVD>2.0.CO;2.

Kaneko, H., I. Yasuda, S. Itoh, and S. Ito. 2021. "Vertical Turbulent Nitrate Flux From Direct Measurements in the Western Subarctic and Subtropical Gyres of the North Pacific." *Journal of Oceanography* 77: 29–44. https://doi.org/10.1007/s10872-020-00576-0.

Karl, D., R. Letelier, L. Tupas, J. Dore, J. Christian, and D. Hebel. 1997. "The Role of Nitrogen Fixation in Biogeochemical Cycling in the Subtropical North Pacific Ocean." *Nature* 388: 533–538. https://doi.org/10.1038/41474.

Karl, D. M., and M. J. Church. 2017. "Ecosystem Structure and Dynamics in the North Pacific Subtropical Gyre: New Views of an Old Ocean." *Ecosystems* 20: 433–457. https://doi.org/10.1007/s10021-017-0117-0.

Kumamoto, Y., M. Aoyama, Y. Hamajima, E. Oka, and A. Murata. 2018. "Time Evolution of Fukushima-Derived Radiocesium in the Western Subtropical Gyre of the North Pacific Ocean by 2017." *Journal of Radioanalytical and Nuclear Chemistry* 318: 2181–2187. https://doi.org/10.1007/s10967-018-6133-5.

Letscher, R. T., F. Primeau, and J. K. Moore. 2016. "Nutrient Budgets in the Subtropical Ocean Gyres Dominated by Lateral Transport." *Nature Geoscience* 9: 815–819. https://doi.org/10.1038/ngeo2812.

Lim, I., C. Sun, J.-H. Lee, J. Kim, and S. Lee. 2023. "Seasonal Variations of Dissolved Rare Earth Elements and Anthropogenic Gadolinium in the Highly Urbanized River Basin, Busan, Korea." *Estuarine, Coastal and Shelf Science* 288: 108359. https://doi.org/10.1016/j.ecss.2023.108359.

Liu, Q., J. Zhang, H. He, et al. 2022. "Significance of Nutrients in Oxygen-Depleted Bottom Waters Via Various Origins on the Mid-Outer Shelf of the East China Sea during Summer." *Science of the Total Environment* 826: 154083. https://doi.org/10.1016/j.scitotenv.2022.154083.

McGillicuddy, D. J., and A. R. Robinson. 1997. "Eddy-Induced Nutrient Supply and New Production in the Sargasso Sea." *Deep Sea Research, Part I: Oceanographic Research Papers* 44: 1427–1450. https://doi.org/10.1016/S0967-0637(97)00024-1.

McGillicuddy, D. J., A. R. Robinson, D. A. Siegel, et al. 1998. "Influence of Mesoscale Eddies on New Production in the Sargasso Sea." *Nature* 394: 263–266. https://doi.org/10.1038/28367.

Meng, S., X. Gong, Y. Yu, et al. 2021. "Strengthened Ocean-Desert Process in the North Pacific Over the Past Two Decades." *Environmental Research Letters* 16: 024034. https://doi.org/10.1088/1748-9326/abd96f.

Metzger, E. J., and H. E. Hurlburt. 1996. "Coupled Dynamics of the South China Sea, the Sulu Sea, and the Pacific Ocean." *Journal of Geophysical Research: Oceans* 101: 12331–12352. https://doi.org/10.1029/95JC03861.

Moffett, J. W. 1990. "Microbially Mediated Cerium Oxidation in Sea Water." *Nature* 345: 421–423. https://doi.org/10.1038/345421a0.

Möller, P., P. Dulski, and M. De Lucia. 2021. "REY Patterns and Their Natural Anomalies in Waters and Brines: The Correlation of Gd and Y Anomalies." *Hydrology* 8: 116. https://doi.org/10.3390/hydrology8030116.

Mouriño-Carballido, B., J. L. Otero Ferrer, B. Fernández Castro, et al. 2021. "Magnitude of Nitrate Turbulent Diffusion in Contrasting Marine Environments." *Scientific Reports* 11: 18804. https://doi.org/10.1038/s41598-021-97731-4.

Nozaki, Y., D.-S. Alibo, H. Amakawa, T. Gamo, and H. Hasumoto. 1999. "Dissolved Rare Earth Elements and Hydrography in the Sulu Sea." *Geochimica et Cosmochimica Acta* 63: 2171–2181. https://doi.org/10.1016/S0016-7037(99)00142-8.

Nozaki, Y., J. Zhang, and H. Amakawa. 1997. "The Fractionation Between Y and Ho in the Marine Environment." *Earth and Planetary Science Letters* 148: 329–340. https://doi.org/10.1016/S0012-821X(97)00034-4.

Pan, Y., W. Fan, T.-H. Huang, S.-L. Wang, and C.-T. A. Chen. 2015. "Evaluation of the Sinks and Sources of Atmospheric CO_2 by Artificial Upwelling." *Science of the Total Environment* 511: 692–702. https://doi.org/10.1016/j.scitotenv.2014.11.060.

Qiu, B., S. Chen, P. Klein, H. Sasaki, and Y. Sasai. 2014. "Seasonal Mesoscale and Submesoscale Eddy Variability Along the North Pacific Subtropical Countercurrent." *Journal of Physical Oceanography* 44: 3079–3098. https://doi.org/10.1175/JPO-D-14-0071.1.

Radic, A., F. Lacan, and J. W. Murray. 2011. "Iron Isotopes in the Seawater of the Equatorial Pacific Ocean: New Constraints for the Oceanic Iron Cycle." *Earth and Planetary Science Letters* 306: 1–10. https://doi.org/10.1016/j.epsl.2011.03.015.

Resplandy, L., M. Lévy, and D. J. McGillicuddy Jr. 2019. "Effects of Eddy-Driven Subduction on Ocean Biological Carbon Pump." *Global Biogeochemical Cycles* 33: 1071–1084. https://doi.org/10.1029/2018GB006125.

Shih, Y.-Y., C.-C. Hung, G.-C. Gong, et al. 2015. "Enhanced Particulate Organic Carbon Export at Eddy Edges in the Oligotrophic Western North Pacific Ocean." *PLoS One* 10: e0131538. https://doi.org/10.1371/journal.pone.0131538.

Singh, S. P., S. K. Singh, V. Goswami, R. Bhushan, and V. K. Rai. 2012. "Spatial Distribution of Dissolved Neodymium and εNd in the Bay of Bengal: Role of Particulate Matter and Mixing of Water Masses." *Geochimica et Cosmochimica Acta* 94: 38–56. https://doi.org/10.1016/j.gca.2012.07.017.

Song, H., W.-J. Shin, J.-S. Ryu, H. S. Shin, H. Chung, and K.-S. Lee. 2017. "Anthropogenic Rare Earth Elements and Their Spatial Distributions in the Han River, South Korea." *Chemosphere* 172: 155–165. https://doi.org/10.1016/j.chemosphere.2016.12.135.

Takahashi, T., S. C. Sutherland, R. Wanninkhof, et al. 2009. "Climatological Mean and Decadal Change in Surface Ocean pCO_2, and Net Sea–Air CO_2 Flux Over the Global Oceans." *Deep Sea Research Part II: Topical Studies in Oceanography* 56: 554–577. https://doi.org/10.1016/j.dsr2.2008.12.009.

Takeda, S., N. Ramaiah, M. Miki, et al. 2007. "Biological and Chemical Characteristics of High-Chlorophyll, Low-Temperature Water Observed Near the Sulu Archipelago." *Deep Sea Research Part II: Topical Studies in Oceanography* 54: 81–102. https://doi.org/10.1016/j.dsr2.2006.08.020.

Tanaka, M., H. Shimizu, and A. Masuda. 1990. "Features of the Heavy Rare-Earth Elements in Seawater." *Geochemical Journal* 24: 39–46. https://doi.org/10.2343/geochemj.24.39.

Taylor, S. R., and S. M. McLennan. 1985. The Continental Crust: Its Composition and Evolution. Blackwell Scientific Publications.

Tomczak, M., and D. G. B. Large. 1989. "Optimum Multiparameter Analysis of Mixing in the Thermocline of the Eastern Indian Ocean." *Journal of Geophysical Research: Oceans* 94: 16141–16149. https://doi.org/10.1029/JC094iC11p16141.

Wen, Z., T. J. Browning, Y. Cai, et al. 2022. "Nutrient Regulation of Biological Nitrogen Fixation Across the Tropical Western North Pacific." *Science Advances* 8: eabl7564. https://doi.org/10.1126/sciadv.abl7564.

Whitmore, L. M., A. Pasqualini, R. Newton, and A. M. Shiller. 2020. "Gallium: A New Tracer of Pacific Water in the Arctic Ocean." *Journal of Geophysical Research: Oceans* 125: e2019JC015842. https://doi.org/10.1029/2019JC015842.

Wilson, C. 2021. "Evidence of Episodic Nitrate Injections in the Oligotrophic North Pacific Associated With Surface Chlorophyll Blooms." *Journal of Geophysical Research: Oceans* 126: e2021JC017169. https://doi.org/10.1029/2021JC017169.

Wu, J., Z. Lee, Y. Xie, et al. 2021. "Reconciling Between Optical and Biological Determinants of the Euphotic Zone Depth." *Journal of Geophysical Research: Oceans* 126: e2020JC016874. https://doi.org/10.1029/2020JC016874.

Yang, G., F. Wang, Y. Li, and P. Lin. 2013. "Mesoscale Eddies in the Northwestern Subtropical Pacific Ocean: Statistical Characteristics and Three-Dimensional Structures." *Journal of Geophysical Research: Oceans* 118: 1906–1925. https://doi.org/10.1002/jgrc.20164.

Yuan, Z., T. J. Browning, R. Zhang, et al. 2023. "Potential Drivers and Consequences of Regional Phosphate Depletion in the Western Subtropical North Pacific." *Limnology and Oceanography Letters* 8: 509–518. https://doi.org/10.1002/lol2.10314.

Yuval, J., and Y. Kaspi. 2020. "Eddy Activity Response to Global Warming-Like Temperature Changes." *Journal of Climate* 33: 1381–1404. https://doi.org/10.1175/JCLI-D-19-0190.1.

Zhang, J., Q. Liu, L. Bai, and T. Matsuno. 2018. "Water Mass Analysis and Contribution Estimation Using Heavy Rare Earth Elements: Significance of Kuroshio Intermediate Water to Central East China Sea Shelf Water." *Marine Chemistry* 204: 172–180. https://doi.org/10.1016/j.marchem.2018.07.011.

Zhang, Y., F. Lacan, and C. Jeandel. 2008. "Dissolved Rare Earth Elements Tracing Lithogenic Inputs Over the Kerguelen Plateau (Southern Ocean)." *Deep Sea Research Part II: Topical Studies in Oceanography* 55: 638–652. https://doi.org/10.1016/j.dsr2.2007.12.029.

Zheng, X.-Y., Y. Plancherel, M. A. Saito, P. M. Scott, and G. M. Henderson. 2016. "Rare Earth Elements (REEs) in the Tropical South Atlantic and Quantitative Deconvolution of Their Non-conservative Behavior." *Geochimica et Cosmochimica Acta* 177: 217–237. https://doi.org/10.1016/j.gca.2016.01.018.

Zhou, K., C. R. Benitez-Nelson, J. Huang, P. Xiu, Z. Sun, and M. Dai. 2021. "Cyclonic Eddies Modulate Temporal and Spatial Decoupling of Particulate Carbon, Nitrogen, and Biogenic Silica Export in the North Pacific Subtropical Gyre." *Limnology and Oceanography* 66: 3508–3522. https://doi.org/10.1002/lno.11895.

Zhu, S. J., J. Zhang, T. Matsuno, et al. 2023. "Quantifying the Water Contribution of Subtropical Mode Water and Related Isopycnal/Diapycnal Water Mixing in the Western Pacific Boundary Current Area Using Radiocesium: A Significant Nutrient Contribution From Subtropical Pacific Gyre to the Marginal Region." *Journal of Geophysical Research: Oceans* 128: e2022JC018975. https://doi.org/10.1029/2022JC018975.

Supporting Information

Additional Supporting Information may be found in the online version of this article.

Submitted 24 October 2024
Revised 31 May 2025
Accepted 26 September 2025